FINAL REPORT: MS Theses

NASA GRANT NUMBER NCC 2-775
Cal Poly Project 5328

Helicopter Approach Capability Using the Differential Global Positioning System

David N. Kaufmann: Graduate Student

A Real-Time Algorithm for Integrating Differential Satellite and Inertial Navigation Information during Helicopter Approach

Ty Hoang: Graduate Student

PI: Daniel J. Biezad

NASA Technical Monitor:
Mr. Harry Swenson
NASA Ames Research Center
Moffett Field, CA. 94035-1000

April 1994

HELICOPTER APPROACH CAPABILITY USING
THE DIFFERENTIAL GLOBAL POSITIONING SYSTEM

A Thesis

Presented to

the Faculty of the Graduate School

California Polytechnic State University, San Luis Obispo

In Partial Fulfillment

of the Requirements for the Degree

Master of Science in Aeronautical Engineering

by

David N. Kaufmann

June 1993

AUTHORIZATION FOR

REPRODUCTION OF MASTER'S THESIS

I grant permission for the reproduction of this thesis in its entirety or any of its parts, without further authorization from me.

_____

Signature

<u>10 May 1993</u>_____

Date

APPROVAL PAGE

TITLE: Helicopter Approach Capability Using the Differential Global Positioning System

AUTHOR: David N. Kaufmann

DATE SUBMITTED: June 1993

Dr. Daniel J. Biezad
Advisor   Signature
Aeronautical Engineering Department
California Polytechnic State University
San Luis Obispo, CA 93407

Harry N. Swenson
Technical Officer   Signature
Aircraft Guidance and Navigation Branch
NASA Ames Research Center
Moffett Field, CA 94035

Dr. Russell M. Cummings
Committee Member   Signature
Aeronautical Engineering Department
California Polytechnic State University
San Luis Obispo, CA 93407

Professor William B. Patterson
Committee Member   Signature
Mechanical Engineering Department
California Polytechnic State University
San Luis Obispo, CA 93407

ABSTRACT

Helicopter Approach Capability Using
the Differential Global Positioning System

by

David N. Kaufmann

The results of flight tests to determine the feasibility of using the Global Positioning System (GPS) in the differential mode (DGPS) to provide high accuracy, precision navigation and guidance for helicopter approaches to landing are presented. The airborne DGPS receiver and associated equipment is installed in a NASA UH-60 Black Hawk helicopter. The ground-based DGPS reference receiver is located at a surveyed test site and is equipped with a real-time VHF data link to transmit correction information to the airborne DGPS receiver. The corrected airborne DGPS information, together with the preset approach geometry, is used to calculate guidance commands which are sent to the aircraft's approach guidance instruments. The use of DGPS derived guidance for helicopter approaches to landing is evaluated by comparing the DGPS data with the laser tracker truth data.

Both standard (3°) and steep (6° and 9°) glideslope straight-in approaches were flown. DGPS positioning accuracy based on a time history analysis of the entire approach was 0.2 m (mean) ±1.8 m (2σ) laterally and -2.0 m (mean) ±3.5 m (2σ) vertically for 3° glideslope approaches, -0.1 m (mean) ±1.5 m (2σ) laterally and -1.1 m (mean) ±3.5 m (2σ) vertically for 6° glideslope approaches and 0.2 m (mean) ±1.3 m (2σ) laterally and -1.0 m (mean) ±2.8 m (2σ) vertically for 9° glideslope approaches.

DGPS positioning accuracy at the 200 ft decision height (DH) on a standard 3° glideslope approach was 0.3 m (mean) ±1.5 m (2σ) laterally and -2.3 m (mean) ±1.6 m (2σ) vertically. These errors indicate that the helicopter position based on DGPS guidance satisfies the International Civil Aviation Organization (ICAO) Category 1 (CAT 1) lateral and vertical navigational accuracy requirements.

ACKNOWLEDGMENTS

TABLE OF CONTENTS

LIST OF TABLES

LIST OF FIGURES

CHAPTER 1

Introduction

GPS Overview

The NAVSTAR GPS is a space-based, navigation satellite system that will provide the user with precise three-dimensional position and velocity information as well as coordinated GPS time continuously, regardless of location, altitude, weather or time of day [1]. GPS is separated into three major segments: 1) the space segment, which is comprised of the earth-orbiting satellite constellation, 2) the control segment, which monitors the health and orbits of the satellites and 3) the user segment, which is comprised of all of the air, land, sea and spaced-based users with GPS receivers.

Space Segment

The space segment, the constellation of earth-orbiting satellites, will consist of 21 satellites plus three active spares, when fully operational in 1994. They will be distributed uniformly in six subsyncronous circular orbital planes providing a minimum of four visible satellites at any one time anywhere on earth. These orbital planes are inclined 55° with respect to the equatorial plane and separated longitudinally by 60°. The satellites orbit at an altitude of 10898 nm and with a period of 12 hours.

Signals from the satellites are transmitted continuously on two L-band frequencies designated L_1 and L_2, where L_1 is 1575.42 MHz and L_2 is 1227.60 MHz. The L_1 frequency is modulated with both the coarse/acquisition (C/A) code and precision (P) code, while the L_2 frequency is modulated only by P code. The C/A code has a frequency of 1.023 MHz and a wavelength of 300 m, with a period of one ms. The P code has a frequency of 10.23 MHz and a wavelength of 30 m, with a period of one week. The structure and composition of the P code signal is classified by the U.S. Department of Defense. In addition, both the L_1 and L_2 frequencies are further modulated by a navigation message which contains GPS time, GPS almanac data, satellite ephemeris

data, satellite health, atmospheric propagation correction data as well as any other information needed by the GPS receiver.

Control Segment

The control segment monitors, and corrects if required, the satellite broadcast signals to ensure a pre-defined accuracy level. In addition, the control segment is responsible for monitoring and controlling the orbits of the satellites, maintaining the GPS time and uplinking necessary information to the satellites three times a day. The control segment, when fully operational, will consist of a Master Control Station (MCS), located at Falcon AFB, Colorado Springs, CO, five monitor stations, one located at the MCS and the other four on the following islands; Hawaii, Kwajalein, Diego Garcia and Ascension and three uplink antennas. The monitor stations allow simultaneous tracking of the complete constellation and relay orbital information, GPS time and any other necessary information to the MCS. The ranging information, acquired by the monitoring stations, is then processed for use in satellite orbit determination and systematic error elimination. The MCS then calculates corrections that are uplinked to the satellites via the three uplink antennas.

User Segment

The user segment is intended for both military and civilian users of the system. In order to use GPS, a receiver is required. The GPS receiver consists of an antenna to capture the GPS signals, an amplifier to boost the power level of the received signals and a digital computer to process the information contained within the signals.

The GPS receiver selects and measures a minimum of four independent satellite signals in order to calculate a three-dimensional position fix. In addition, three-dimensional velocity and GPS time is calculated. The GPS design specifications require the calculated position to be accurate to within 15 m Spherical Error Probable (SEP), the calculated velocity to be accurate to within 0.1 m/s (1σ) and the GPS time to be within

100 ns (1σ) [2]. Since the GPS information is output in the World Geodetic System, 1984 (WGS-84) Earth-Centered, Earth-Fixed (ECEF) coordinate system, military and civilian position data can be standardized on a worldwide basis.

Position Solution

The GPS receiver position fix is accomplished by means of passive tri-lateration. Since the positions of the satellites are known at all times, the GPS receiver position is determined by measuring the distance between the receiver and a minimum of four satellites. The satellite atomic cesium clocks are kept synchronized to the GPS time by the MCS. The less accurate clocks contained within the GPS receivers are not. Therefore, the measurement of the signal's time of travel will be in error by an amount equal to the difference between the atomic time standard maintained by the satellite and the time maintained by the GPS receiver. This error produces an inaccurate range measurement between the GPS receiver and each satellite it is receiving, known as "pseudorange". In addition to the above time difference error, a satellite clock error as well as ionospheric and tropospheric delays are present. However, the effect of the satellite clock error is negligible for the typical navigation solution. In addition, this error is indistinguishable from the ionospheric and tropospheric delays. Actual offsets of the satellite clocks are approximated by polynomials in time and transmitted as part of the satellite signal to the user for the correction of the measured pseudorange. The ionospheric and tropospheric delays can be calculated on the basis of ionospheric and tropospheric models. Therefore, for each pseudorange measurement, an equation can be derived that relates the measurement to the satellite position and the unknown quantities of GPS receiver position and GPS receiver clock error. Since four unknown quantities exist, a minimum of four pseudorange measurements must be taken and solved simultaneously to determine the three-dimensional GPS receiver position. Mathematically, the pseudorange is defined as [3]:

$$p_i = \sqrt{(X - x_i)^2 + (Y - y_i)^2 + (Z - z_i)^2} - c(dT) \qquad (1)$$

where:

p_i is the pseudorange measurement to satellite i

X,Y,Z is the GPS receiver position in the ECEF coordinate system

x_i, y_i, z_i is the position of satellite i in the ECEF coordinate system

c is the speed of light (299,792,458 m/s)

dT is the GPS receiver clock error

The effect of the GPS receiver clock error and the way in which its measurement is used to calculate the true position of the GPS receiver is shown in Figure 1.
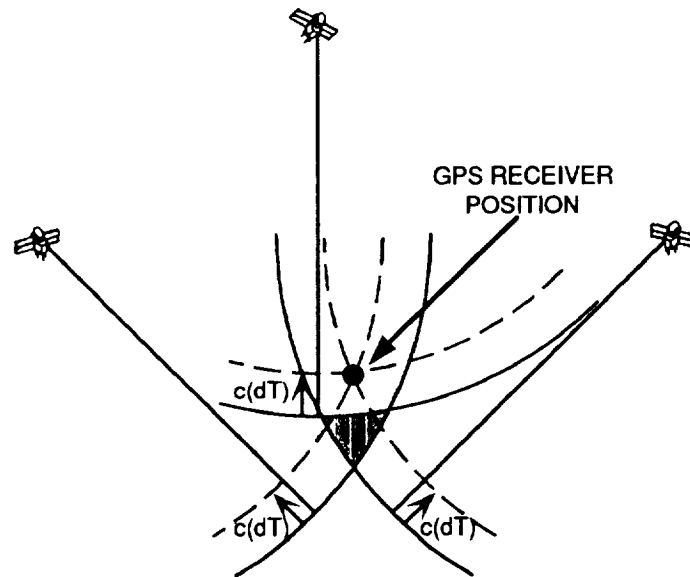
Figure 1

GPS Receiver Clock Error And Calculation Of True Position

This figure illustrates that the pseudorange radii do not converge at a single point but instead enclose the shaded triangular area. However, if the range value equivalent to c(dT) is added to (or subtracted from, if the case warrants) the pseudorange, then the radii converge to a single point, the GPS receiver position. Figure 1 represents only a two-dimensional case in which all three of the satellites and the GPS receiver lie in the same plane. However, the same logic applies to the three-dimensional case with four satellites.

Geometric Effects

GPS receiver clock error is not the only contributor to the position error. The relative geometry of the satellites being tracked and the GPS receiver also affects the position accuracy. Therefore, in order to determine the accuracy available from the satellites being tracked as a function of their geometry, the Dilution of Precision (DOP) values must be calculated [1].

The DOP is composed of Position Dilution of Precision (PDOP), which reflects the dilution of precision in three-dimensional position; Horizontal Dilution of Precision (HDOP), which reflects the dilution of precision in the two horizontal dimensions; Vertical Dilution of Precision (VDOP), which reflects the dilution of precision in the vertical dimension; and Time Dilution of Precision (TDOP), which reflects the dilution of precision in time, i.e., in the estimate of the range error due to the GPS receiver clock error. Geometric Dilution of Precision (GDOP) is a composite value composed of both the position and time DOP. Since the magnitude of the range error due to the GPS receiver clock error is multiplied by the DOP values to obtain the overall position accuracy, small DOP values are desirable [1]. The most frequently used measure of geometric performance is PDOP, which when multiplied by the range error due to the GPS receiver clock error determines the position error. Figure 2 relates satellite geometry to PDOP values.

GOOD (LOW) PDOP

POOR (HIGH) PDOP
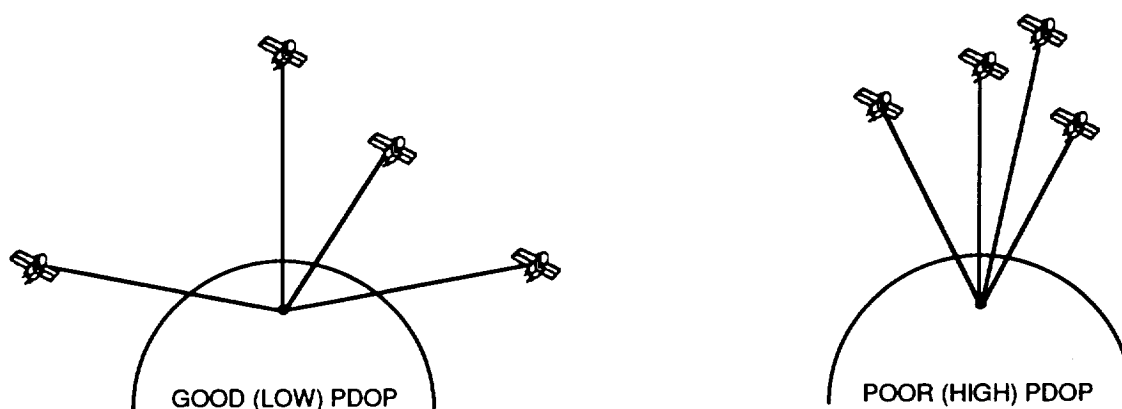
Figure 2

PDOP As A Function Of Satellite Geometry

DGPS Concept

DGPS represents a straight-forward method to significantly improve the accuracy of GPS. The general principle of DGPS is that by having a GPS receiver at a pre-surveyed location, the true values of the location are compared against the measured values, and the resulting pseudorange and pseudorange-rate difference corrections are sent real-time, to be applied to the airborne GPS receiver. This real-time uplink of the pseudorange and pseudorange-rate difference corrections enables the airborne GPS receiver to calculate its position relatively free of measurement errors due to ionospheric delay, tropospheric delay, ephemeris uncertainties, satellite clock error and selective availability (SA), intentional degradation of the C/A signal. SA is accomplished by the degradation of the broadcast ephemeris data (GPS orbits and clock offsets) and by the systematic destabilization of the GPS oscillator. The latter generates an irregularly changing error in the pseudorange and pseudorange-rate values. All of these errors are either eliminated or significantly reduced since they are common to both GPS receivers.

DGPS research at the NASA Ames Research Center was initiated in the early 1980's when a C/A code, single channel sequencing DGPS system was developed and flight tested on a NASA SH-3G helicopter [4-7]. The objective of the tests were to evaluate the use of DGPS to support helicopter terminal approach operations. Final approach positioning accuracy was 5.2 m (mean) ±8.0 m (2σ) laterally and -7.7 m (mean) ±7.0 m (2σ) vertically. The use of barometric and radar altimeters to enhance the vertical axis positioning accuracy yielded 5.0 m (mean) ±6.0 m (2σ) vertically and 5.0 m (mean) ±4.0 m (2σ) vertically, respectively [5,7]. The time lags due to the satellite sequencing were too great for real-time guidance and navigation. However, the positioning accuracy attained during these tests demonstrated the potential of DGPS for terminal approach operations.

Recent fixed-wing DGPS terminal approach and landing flight tests conducted at the NASA Ames Research Center yielded positioning accuracy of 0.1 m (mean) ±1.8 m (2σ) laterally and -0.8 m (mean) ±6.6 m (2σ) vertically, using P code GPS receivers [8]. Thus, a DGPS based guidance and navigation system has the potential to significantly enhance the unique capabilities of the helicopter, as well as improving pilot situational awareness. Specific helicopter missions that would benefit from such a system are:

1. Low altitude operations

2. Remote area landing

3. Search and rescue operations

4. Inter-city operations

The above missions could be carried out regardless of weather conditions, time of day or location

The use of C/A code DGPS in real-time to provide high accuracy, precision navigation and guidance for helicopter approaches to landing is the subject of this thesis.

The objective is to evaluate, through flight test, C/A code DGPS positioning accuracy during helicopter approaches to landing.

So far, this thesis has described the GPS and the concept behind DGPS. Chapter 2 discusses the airborne and ground-based systems required to perform the flight tests. Chapter 3 describes the derivation of the DGPS-based guidance solution while Chapter 4 outlines the flight test procedures. Chapter 5 presents the flight test results and Chapter 6 draws conclusions from the results obtained. Sample flight test data and processed data are included in the Appendix, as well as the computer code and instructions used to process the data. In addition, the airborne and ground-based system checklists are included.

—

CHAPTER 2

Test Equipment And Facilities

<u>Equipment Description</u>

The operational layout of the facilities for the flight tests is shown in Figure 3, which

shows the various components involved. These include the NASA UH-60 helicopter

with the Ashtech GPS receiver operating onboard, the ground-based Ashtech GPS

receiver and antenna located at a pre-surveyed test location and the laser tracker used to

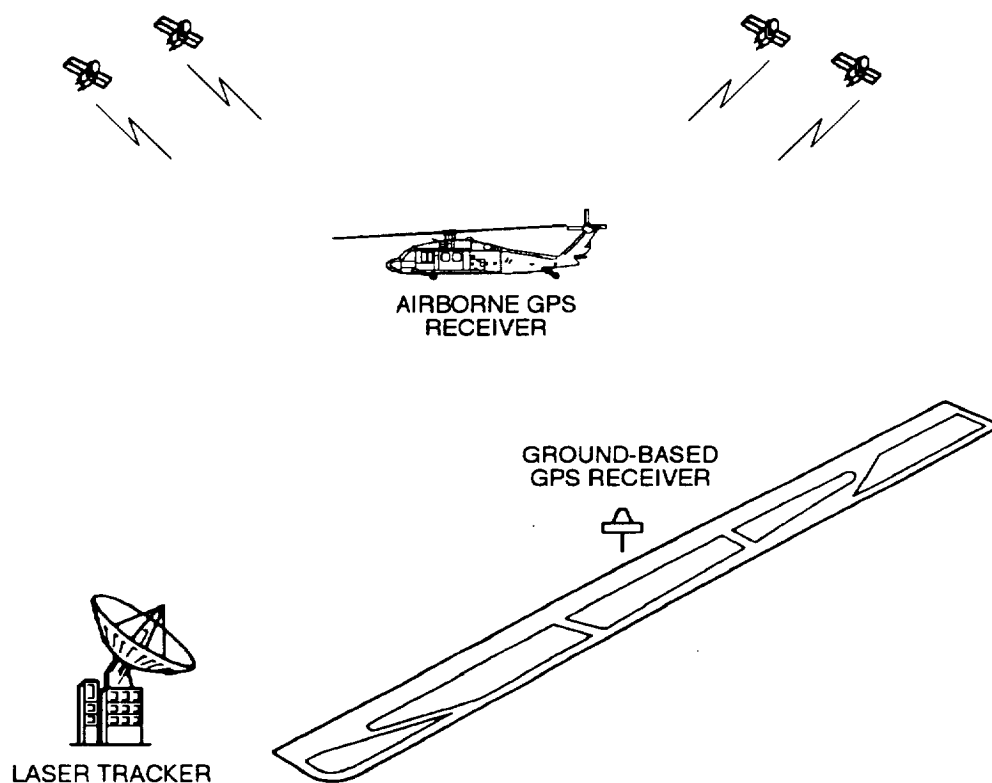provide the true position and velocity of the aircraft during the flight tests.

AIRBORNE GPS
RECEIVER

GROUND-BASED
GPS RECEIVER

LASER TRACKER

Figure 3

Flight Test Facilities

Airborne System

The test aircraft is a modified UH-60 Black Hawk helicopter located at the NASA Ames Research Center (See Figure 4). During the flight tests, two pilots are required to fly the aircraft and operate the aircraft systems. In addition, a research engineer is required to operate the airborne test equipment and to coordinate operations between the airborne and ground-based systems. The airborne test equipment consists of a Ashtech Model XII 12 channel C/A code GPS receiver, a Maxon/Ashtech SM 3010 VHF telemetry uplink receiver, a Litton LN-93 ring laser gyro Inertial Navigation System (INS) (used only for post-processing data collection), a 486 processor based Data Acquisition/Navigation Computer (DAC) and an interface to the aircraft's standard approach guidance instruments (See Figure 5). In addition, a Tandy 102 laptop computer is used to control both the data acquisition and navigation functions. The GPS antenna is located at the rear of the aircraft on top of the vertical stabilizer, adjacent to the tail rotor. The telemetry uplink antenna is located on the bottom of the aircraft approximately midway between the main and tail landing gear. A laser reflector is mounted on both the right and left sponsons for position tracking during the approaches to landing.

The DAC collects GPS position data at a rate of 2 Hz via a RS-232 connection and INS Euler angle data at a rate of 64 Hz via a 1553B data bus. In addition, a precise GPS time pulse is sent to the DAC at a rate of 1 Hz via a digital line. GPS time differs from Universal Coordinated Time (UTC), by not adjusting for leap seconds at periodic end-of-year intervals. Such adjustments in GPS time would disrupt the continuous availability of the satellites for navigation purposes. This time pulse is used to time-tag the INS data to that of the GPS time, via the IRIG-B time, which is derived from GPS time and broadcast from the test site. The telemetry uplink receiver is connected to the GPS receiver by a RS-232 connection and receives the pseudorange and pseudorange-rate difference corrections at a rate of approximately 0.5 Hz. The computer-derived lateral

and vertical deviations are output to the approach guidance instruments at a rate of 2 Hz via a RS-232 connection. All airborne data collected from each approach is stored on a removable 44 MB Syquest hard drive for post-flight analysis.
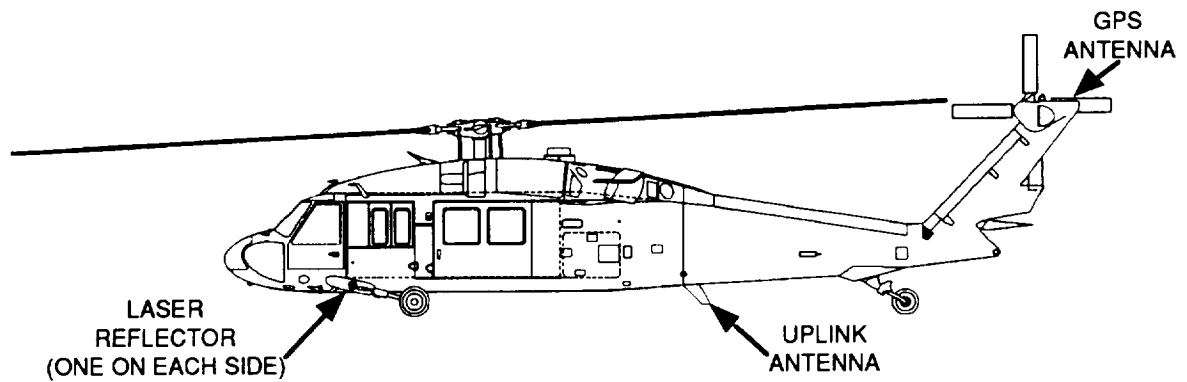
Figure 4

NASA UH-60 Helicopter
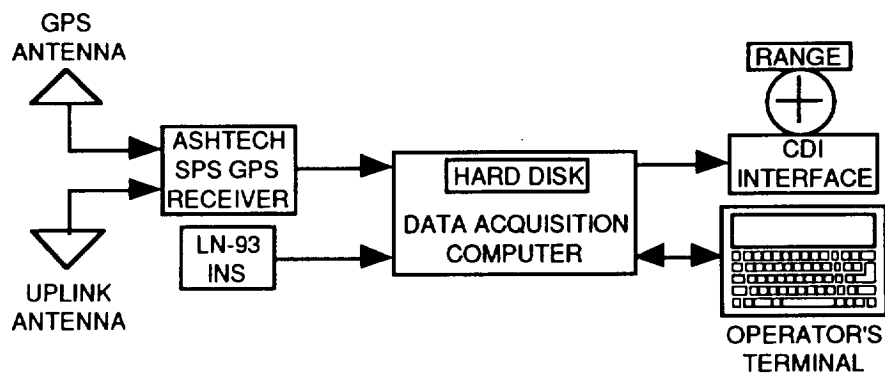
Figure 5

Airborne System

The DGPS based guidance is displayed in the cockpit (using standard Instrument Landing System (ILS) type localizer and glideslope instruments) using a special interface unit that converts computer-derived lateral and vertical deviations from a nominal localizer and glideslope to simulated ILS localizer and glideslope signals, respectively [9].

Ground-Based Reference System

The ground-based test equipment consists of an identical Ashtech Model XII GPS receiver, a Maxon/Ashtech SM 3010 VHF telemetry uplink transmitter and a laser tracker (See Figure 6). A research engineer monitors the ground-based test equipment and is in two-way radio contact with the aircraft at all times. The telemetry uplink transmitter is connected to the GPS receiver by a RS-232 connection and broadcasts the pseudorange and pseudorange-rate difference corrections at a rate of approximately 0.5 Hz. The GPS receiver antenna is permanently positioned at a pre-surveyed test location that allows for unobstructive viewing of the satellites. The telemetry uplink antenna is positioned so as to have line-of-sight with the aircraft throughout the flight test pattern. The laser tracking data is time-tagged with the IRIG-B time prior to being recorded.
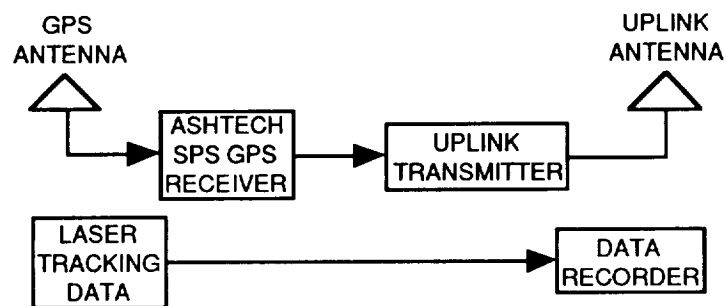
Figure 6

Ground-Based Reference System

Laser Tracking System

All flight tests were conducted at Crows Landing NAS, Crows Landing, CA, located approximately 50 miles east of Moffett Field NAS. The NASA test facility at Crows Landing NAS includes two Nike X-band monopulse radar trackers and one precision NiYag laser tracker. The laser tracker provides precise aircraft range, azimuth and elevation and is used to provide the reference or truth data by tracking the reflectors mounted on the aircraft. Laser range accuracy is nominally ±0.3 m out to approximately 9 km; azimuth and elevation accuracy are nominally ±0.2 mrad. During the terminal part of the approach this corresponds to position errors of less than 0.5 m in each axis. Note that these accuracies are of the same order of magnitude as the expected DGPS position accuracies. The laser tracker was calibrated each morning prior to a test flight. Refer to Appendix A for a geographic description of the test facilities at Crows Landing NAS.

CHAPTER 3

DGPS Based Guidance Solution

The airborne GPS receiver calculates its position (m) and velocity (m/s) in the ECEF coordinate system at a rate of 2 Hz. In this reference frame, the origin is located at the earth's center of mass, the X_E axis is oriented through the equator at the Greenwich meridian, the Y_E axis lies 90° to the east through the equator and the Z_E axis is oriented up through the North Pole. The navigation function of the DAC converts these positions and velocities into the local Runway Coordinate System (RCS) reference frame to provide guidance and for post-flight evaluation. In the RCS reference frame, the origin is located at the aim point to the runway being flown to, the X_R axis is oriented parallel to and down the runway, the Y_R axis lies 90° to the right and the Z_R axis is oriented down, normal to the runway. Refer to Appendix A for a full description of the RCS reference frame at Crows Landing NAS.

The first step in the conversion is to transform the WGS-84 geodetic coordinates of the aim point being flown to into the ECEF coordinate system. Since the earth rotates, it assumes the shape of a sphere that is flattened at the poles and bulging at the equator. Therefore, the earth can be modeled by an ellipsoid of revolution formed by rotating an ellipse around its minor axis [10]. Figure 7 shows the ellipsoid of revolution and the associated ECEF reference frame. As discussed above, the ECEF coordinates (X_E, Y_E, Z_E) originate at the earth's center of mass; the X_E axis is oriented through the equator at the Greenwich meridian, the Y_E axis lies 90° to the east through the equator and the Z_E axis is oriented up through the North Pole, which coincides with the ellipsoid semi-minor axis. The ellipsoidal normal through a point P intersects the Z_E axis, but does not pass through the center of mass, due to the flattening of the ellipsoid. The length of the ellipsoidal normal from the surface of the ellipsoid to the point P is called the geodetic height, h. The angle between the ellipsoidal normal and the equatorial plane is the geodetic latitude,

φ. Any intersection of the ellipsoid of revolution with a plane containing the Z_E axis is an ellipse called the ellipsoidal meridian. The geodetic longitude, λ, is the angle between two meridional planes oriented⟨clockwise from the X_E axis. Therefore, the geodetic coordinates (φ,λ,h) completely describe the position of a point ʷᴿᵀ on the earth.
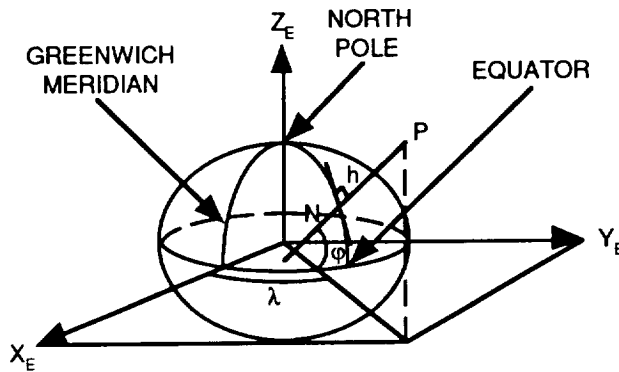
Figure 7

Earth Ellipsoid Of Revolution

The relationship between the geodetic coordinates (φ,λ,h) of the Crows Landing NAS Runway 35 Aim Point (AP) and the ECEF coordinates (X_E,Y_E,Z_E) is as follows [10]:

$$\begin{bmatrix} AP_{X_E} \\ AP_{Y_E} \\ AP_{Z_E} \end{bmatrix} = \begin{bmatrix} (N+h)\cos\varphi\cos\lambda \\ (N+h)\cos\varphi\sin\lambda \\ (N(1-e^2)+h)\sin\varphi \end{bmatrix} \tag{2}$$

where:

$N = \dfrac{a}{\sqrt{1-e^2\sin^2\varphi}}$, the radius of the earth ellipsoid of revolution

$$e = \sqrt{\frac{2(a-b)}{a} - \frac{(a-b)^2}{a^2}} \text{, the eccentricity of the earth ellipsoid of revolution}$$

a is the semi-major axis of the earth ellipsoid of revolution (6378137.0 m)

b is the semi-minor axis of the earth ellipsoid of revolution (6356752.3141 m)

φ is the geodetic latitude of the Runway 35 Aim Point (37.41335361° N)

λ is the geodetic longitude of the Runway 35 Aim Point (121.1082725° W)

h is the geodetic height of the Runway 35 Aim Point (12.4 m)

All of the numerical values above are valid only for the WGS-84 earth ellipsoid of revolution.

Once the coordinates of the aim point in the ECEF reference frame are calculated, the difference between the airborne GPS receiver antenna position and the aim point can be determined as follows:

$$\begin{bmatrix} \Delta_{X_E} \\ \Delta_{Y_E} \\ \Delta_{Z_E} \end{bmatrix} = \begin{bmatrix} A_{X_E} \\ A_{Y_E} \\ A_{Z_E} \end{bmatrix} - \begin{bmatrix} AP_{X_E} \\ AP_{Y_E} \\ AP_{Z_E} \end{bmatrix} \tag{3}$$

where:

$\begin{bmatrix} A_{X_E} \\ A_{Y_E} \\ A_{Z_E} \end{bmatrix}$ is the position of the airborne GPS receiver antenna in the ECEF reference

    frame

$\begin{bmatrix} AP_{X_E} \\ AP_{Y_E} \\ AP_{Z_E} \end{bmatrix}$ is the position of the Runway 35 Aim Point in the ECEF reference frame

All airborne positions, and therefore all position differences with respect to the Runway 35 Aim Point, are based upon the position of the airborne GPS receiver antenna, which is the origin of the navigation solution.

After the ECEF position difference is calculated, the airborne GPS receiver antenna position in the ECEF reference frame is transformed into the RCS reference frame as follows:

$$\begin{bmatrix} A_{X_R} \\ A_{Y_R} \\ A_{Z_R} \end{bmatrix} = \begin{bmatrix} C_E^R \end{bmatrix} \begin{bmatrix} \Delta_{X_E} \\ \Delta_{Y_E} \\ \Delta_{Z_E} \end{bmatrix}$$

(4)

where:

$C_E^R = \begin{bmatrix} C_V^R \end{bmatrix}\begin{bmatrix} C_E^V \end{bmatrix}$, the transformation matrix from the ECEF reference frame to the RCS reference frame

$$C_E^V = \begin{bmatrix} -\sin\varphi\cos\lambda & -\sin\varphi\sin\lambda & \cos\varphi \\ -\sin\lambda & \cos\lambda & 0 \\ -\cos\varphi\cos\lambda & -\cos\varphi\sin\lambda & -\sin\varphi \end{bmatrix}$$, the transformation matrix from the ECEF

reference frame to the Vehicle-Carried Vertical (VCV) reference frame, where the origin is located at the Runway 35 Aim Point, the X_V axis is oriented towards True North, the Y_V axis is oriented towards True East and the Z_V axis is oriented down, normal to the runway

φ is the geodetic latitude of the Runway 35 Aim Point ($37.41335361°$ N)

λ is the geodetic longitude of the Runway 35 Aim Point ($121.1082725°$ W)

h is the geodetic height of the Runway 35 Aim Point (12.4 m)

$$C_V^R = \begin{bmatrix} \cos H & \sin H & 0 \\ -\sin H & \cos H & 0 \\ 0 & 0 & 1 \end{bmatrix}$$, the transformation matrix from the VCV reference frame

to the RCS reference frame

H is the Runway 35 True Heading ($10.099°$)

The GPS receiver velocity is transformed, by the DAC, from the ECEF reference frame to the RCS reference frame in the same manner as the GPS receiver position, both

calculated at a rate of 2 Hz, the rate at which the GPS receiver calculates its position and velocity.

With the GPS receiver position solution in the RCS reference frame, approach guidance commands are calculated, based on the aircraft's angular deviation from the nominal localizer and glideslope selected, and sent to the aircraft's approach guidance instruments as simulated ILS localizer and glideslope guidance at a rate of 2 Hz.

The localizer error is calculated as follows:

$$LOC_{Error} = \tan^{-1} \frac{A_{Y_R}}{-A_{X_R}} \tag{5}$$

If the aircraft is to the right of the runway centerline, a positive localizer error is generated and a fly-left command is sent to the aircraft's standard approach guidance instruments proportional to the amount off course. Correspondingly, if the aircraft is to the left of the runway centerline, a negative localizer error is generated and a fly-right command is sent to the aircraft's standard approach guidance instruments proportional to the amount off course. Figure 8 illustrates the localizer error geometry.

The glideslope error is calculated as follows:

$$GS_{Error} = \tan^{-1} \frac{-A_{Z_R}}{\sqrt{(A_{X_R})^2 + (A_{Y_R})^2}} - GS_{Selected} \tag{6}$$

If the aircraft is above the selected glideslope, a positive glideslope error is generated and a fly-down command is sent to the aircraft's standard approach guidance instruments proportional to the amount off glideslope. Correspondingly, if the aircraft is below the selected glideslope, a negative glideslope error is generated and a fly-up command is sent to the aircraft's standard approach guidance instruments proportional to the amount off glideslope. Figure 9 illustrates the glideslope error geometry.
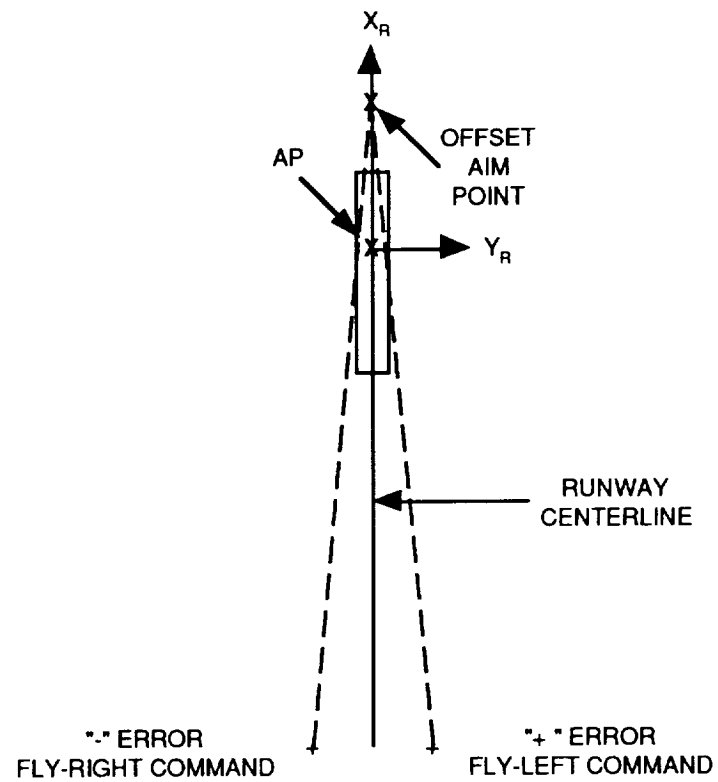
Figure 8
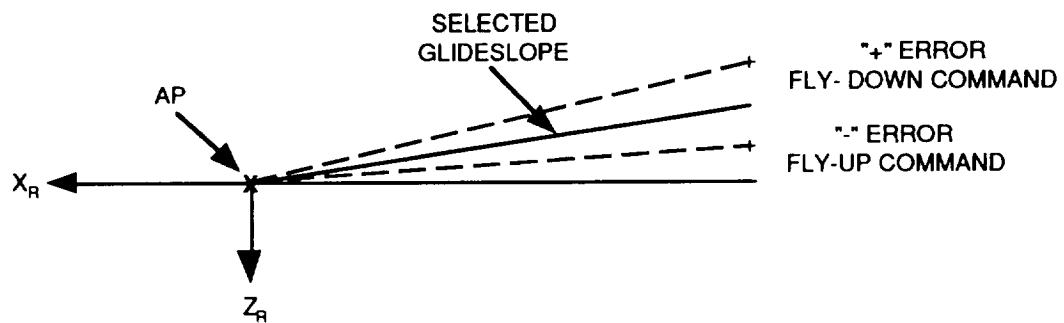
Localizer Error Geometry

Figure 9

Glideslope Error Geometry

Previous flight tests involving helicopters flying steep approaches to landing displayed the need to provide a lateral course width (full-scale lateral deflection, ±2 dots on the Course Deviation Indicator (CDI),) of ±350 ft at the DH [11]. In addition, the flight tests also indicated the need to provide vertical angular glideslope widths of ±1°, ±2° and ±3° for the 3°, 6° and 9° glideslopes, respectively. This corresponds to a full-scale vertical deflection, ±2 dots on the CDI. These values were incorporated into the DGPS-based guidance solution in order to give the non-standard approaches (6° and 9° glideslopes) the sensitivity of the standard approach (3° glideslope).

To achieve a ±350 ft lateral course width at the DH, an offset aim point (OAP) for the localizer angular course width is utilized as the reference point for the angular deviations from the nominal localizer selected (See Figure 10). Since selecting a different glideslope changes the horizontal range (HR) between the DH and the aim point, a pre-defined OAP for each of the three glideslopes is utilized, depending upon which glideslope is selected for the approach.

To achieve the vertical angular glideslope widths of ±1°, ±2° and ±3° for the 3°, 6° and 9° glideslopes, respectively, the aim point is utilized as the reference point for the angular deviations from the nominal glideslope selected (See Figure 11). Since selecting a different glideslope changes the vertical angular glideslope width, a pre-defined glideslope sensitivity (°/dot) for each of the three glideslopes is utilized, depending upon which glideslope is selected for the approach.

For all guidance and navigation calculations, a flat earth model was assumed, therefore, neither Coriolis or centripetal accelerations were included. In addition, gravity was assumed to be of a constant value. These assumptions are valid since the airspeeds involved are relatively slow (80 Knots Indicated Air Speed (KIAS)), and the flight tests are conducted at one location at relatively low altitudes (3000 ft Mean Sea Level (MSL) and below).

OAP

GS	X (ft)	HR (ft)
3°	7069.8975	954.0568
6°	7072.5184	951.4364
9°	7076.8921	947.0627

X

2.5° 2.5°

AP

HR

350 ft   350 ft

DH
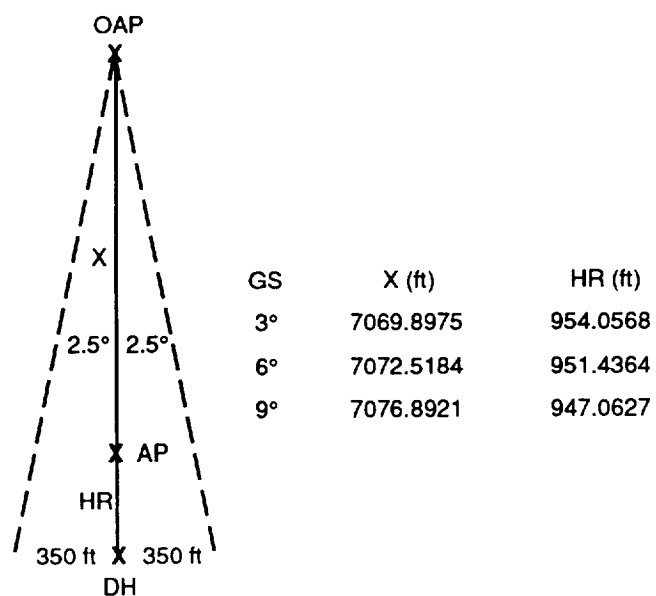
Figure 10

Localizer Geometry

VERTICAL
COURSE
WIDTH

GS

AP   DH

GS	VERTICAL COURSE WIDTH	GS SENSITIVITY
3°	± 1°	0.5°/dot
6°	± 2°	1.0°/dot
9°	± 3°	1.5°/dot
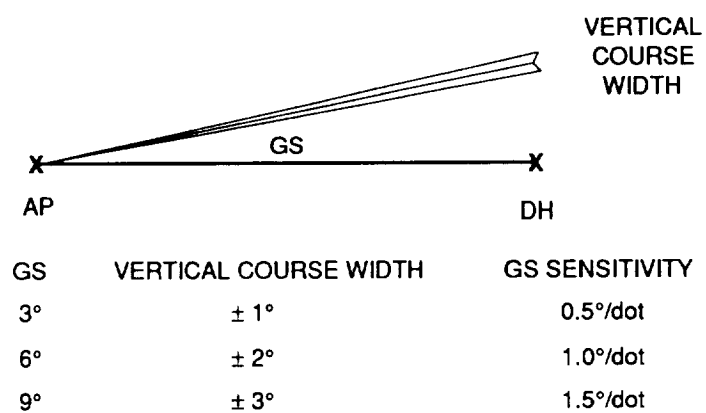
Figure 11

Glideslope Geometry

CHAPTER 4

Flight Test Procedures

Standard (3°) and steep (6° and 9°) glideslope straight-in approaches were used to evaluate helicopter approaches to landing. The 3° glideslope approach was flown at 110 KIAS while the 6° glideslope approach was flown at 85 KIAS and the 9° glideslope approach was flown at 65 KIAS. These airspeeds were chosen to keep the aircraft's rate of descent less than 1000 ft/min. Fourteen separate approaches for each of the three glideslopes were flown for a total of 42 approaches. Throughout all of the approaches, the aircraft was tracked via the laser tracker. All flights were scheduled so that a minimum of five satellites were in view at all times and that the PDOP was less than a value of six.

The overall flight path is a rectangular pattern consisting of four basic components; the crosswind leg, the downwind leg, the base leg and the final approach (See Figure 12). The climbing turn to crosswind is initiated upon reaching the departure end of the active runway and is flown until reaching the downwind leg. The downwind leg is offset 1 nm to the right of the active runway and is flown at the same altitude as the glideslope intercept altitude. The turn to base is initiated at 5.1 nm, which is abeam the Initial Approach Fix (IAF), and is the point where the data collection begins. The base leg is flown so that the aircraft is positioned at the IAF ready to begin the final approach. It is the final approach segment that is of primary interest to this research.

All approaches were initiated at the IAF, located 5 nm out from the aim point along the active runway heading, with the aircraft established on speed, on course, and at the hard altitude associated with the glideslope to be intercepted (1100 ft MSL, 2100 ft MSL and 3000 ft MSL for the 3°, 6° and 9° glideslopes respectively). Upon crossing the IAF, the aircraft is flown inbound to the Final Approach Fix (FAF), located 3 nm out from the aim point along the active runway heading. It is at the FAF that the aircraft intercepts the

appropriate glideslope and flys the approach down to the DH corresponding to the glideslope just flown (190 ft MSL, 240 ft MSL and 290 ft MSL for the 3°, 6° and 9° glideslopes respectively). After descending through the DH, a go-around is initiated at which time the aircraft is flown back to the IAF to set up for another approach. A graphical depiction of the final approach segment is illustrated in Figure 13.
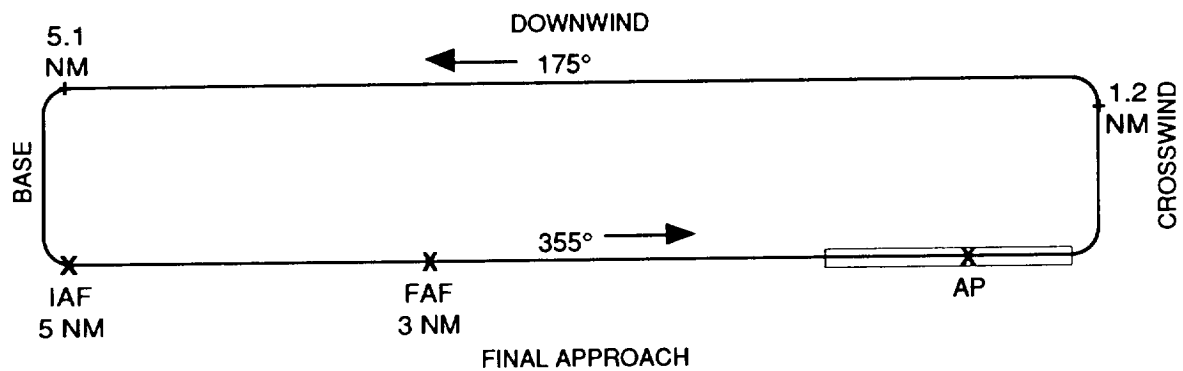

Figure 12

Runway 35 Flight Test Path

GPS (STRAIGHT-IN) RWY 35

RESTRICTED USE
EXPERIMENTAL ONLY

CROWS LANDING NALF (NRC)
CROWS LANDING, CALIFORNIA

CASTLE APP CON
126.5 287.1
CROWS LANDING TWR
125.05 328.1
NASA CON
123.225 382.6

COPTER GPS ONLY
VMC ONLY

AIM POINT 37° 24.8012'
121° 06.4964'
141 ft MSL

LOC
108.1

355°

FAF (3 NM) 37° 21.8572'
121° 07.1549'

IAF (5 NM) 37° 19.8944'
121° 07.5939'

GS (°)	DH (ft MSL)	RECOMENBD KIAS	ROD (fpm)
3	190	80	423
6	240	80	845
9	290	60	948

FAF
(3 NM)

IAF
(5 NM)

355°

3000

2100

1100

9° GS
6° GS
3° GS

355°

AIM
POINT

GPS (STRAIGHT-IN) RWY 35

37° 24' N
121° 06' W

CROWS LANDING NALF (NRC)
CROWS LANDING, CALIFORNIA

Figure 13

Runway 35 Final Approach

CHAPTER 5

Flight Test Results

Data Base Summary

Approaches to be evaluated were chosen based upon the following criteria: 1) continuous tracking of a minimum of four common satellites by both the airborne and ground-based receivers, 2) good satellite geometry (PDOP less than six) and 3) valid laser tracking data.

A time history statistical analysis of the position error during the approach was the primary measure of the DGPS performance. Three-axis position errors for each approach were calculated by taking the difference between the DGPS position (in the RCS reference frame) with the laser tracking data (also in the RCS reference frame). In order to calculate the position errors, the laser tracker truth data position at the laser reflector was transformed to the GPS receiver antenna location as follows:

$$\begin{bmatrix} AL_{X_R} \\ AL_{Y_R} \\ AL_{Z_R} \end{bmatrix} = \begin{bmatrix} L_{X_R} \\ L_{Y_R} \\ L_{Z_R} \end{bmatrix} - \begin{bmatrix} C_V^R \end{bmatrix}\begin{bmatrix} C_2^V \end{bmatrix}\begin{bmatrix} C_3^2 \end{bmatrix}\begin{bmatrix} C_B^3 \end{bmatrix}\begin{bmatrix} \Delta_{X_B} \\ \Delta_{Y_B} \\ \Delta_{Z_B} \end{bmatrix} \tag{7}$$

where:

$$\begin{bmatrix} \Delta_{X_B} \\ \Delta_{Y_B} \\ \Delta_{Z_B} \end{bmatrix} = \begin{bmatrix} 12.9540m \\ 1.4224m \\ 3.2385m \end{bmatrix}$$, the location of the right laser reflector with respect to the GPS

receiver antenna (See Appendix A), in the aircraft body (AB) reference frame, where the origin is located at the aircraft's center of gravity (CG), the X_B axis is oriented forward along the roll axis of inertia, the Y_B axis is oriented to the right along the pitch axis of inertia and the Z_B axis is oriented down along the yaw axis of inertia.

$$C_B^3 = \begin{bmatrix} 1 & 0 & 0 \\ 0 & \cos\Phi & -\sin\Phi \\ 0 & \sin\Phi & \cos\Phi \end{bmatrix}$$, the transformation matrix about the roll axis of inertia

$$C_3^2 = \begin{bmatrix} \cos\Theta & 0 & \sin\Theta \\ 0 & 1 & 0 \\ -\sin\Theta & 0 & \cos\Theta \end{bmatrix}$$, the transformation matrix about the pitch axis of inertia

$$C_2^V = \begin{bmatrix} \cos\Psi & -\sin\Psi & 0 \\ \sin\Psi & \cos\Psi & 0 \\ 0 & 0 & 1 \end{bmatrix}$$, the transformation matrix about the yaw axis of inertia

$$C_V^R = \begin{bmatrix} \cos H & \sin H & 0 \\ -\sin H & \cos H & 0 \\ 0 & 0 & 1 \end{bmatrix}$$, the transformation matrix from the VCV reference frame

to the RCS reference frame

H is the Runway 35 True Heading (10.099°)

The GPS receiver antenna was used as the origin of the navigation solution and therefore, all position errors are based off this location.

Flight tests were conducted on 11 February 1993, 2 April 1993 and 12 April 1993. SA was on during the flight tests. Seven 3°, eight 6° and six 9° glideslope approaches (out of a total of 42), which were flown on the three days with various satellite combinations, were chosen for the statistical analysis. The approaches that were not chosen for the statistical analysis had either airborne or laser tracker data that was incorrectly time-tagged or had incomplete laser tracker data.

<u>Laser Tracker Validation</u>

To verify the post-processing algorithm which transforms the laser tracker truth data to the RCS reference frame, processed data was compared to surveyed position data. Static calibration data was collected prior to each flight by placing the aircraft laser reflector over a known test point on the aircraft parking ramp (See Appendix A). Data

collected at the test point location was transformed into the RCS reference frame in real-time and compared to the surveyed position. Any error greater than 0.5 m in any axis would require that the laser be re-calibrated and verified prior to the flight test. Laser calibration is verified prior to each flight test by taking measurements to several reflectors permanently installed at surveyed locations around the location.

Laser Tracker Reference Results

Figures 14 and 16 show a sample 3° glideslope approach illustrating both DGPS and laser tracker lateral and vertical position with respect to the AP in the RCS reference frame. Note the lateral position angular bias in Figure 14. This is most likely due to the fact that the CDI was not calibrated accurately enough to the computer-derived lateral guidance commands. This angular bias of approximately -0.25° was apparent in all of the approaches evaluated. The lateral and vertical position errors for the same sample approach are shown in Figures 15 and 17. The lateral position error jump at 2500 m is due to laser tracking ambiguities between the right and left laser reflectors (See Figure 15).

Composite lateral and vertical position errors are shown for all of the 3°, 6° and 9° glideslope approaches in Figures 18 through 23. Note that the lateral position error is consistently smaller than the vertical position error, as would be expected. The lateral position error bounds show a slight trend towards increased accuracy as the range decreases. Since the DGPS position accuracy is not a function of the aircraft position during the approach, a possible explanation would be that the laser tracker is more accurate at the shorter ranges. Figures 19, 21 and 23 display large vertical position error bounds at the beginning of the approaches. Again this is most likely due to the inaccuracy of the laser tracker at extended ranges.

Note the set of data points diverging away from the zero error line at approximately 2000 m in Figure 19. This divergence is due to the interruption of the pseudorange and

pseudorange-rate difference correction uplink to the aircraft on flight number 3092-308 and displays the effects of SA. These diverging data points correspond to an interruption that lasted for 44 sec and were not used in any position error statistical analysis. Since the error due to SA is a function of time, the pseudorange and pseudorange-rate difference corrections are time dependent. Therefore the age of the pseudorange and pseudorange-rate difference corrections is critical to the accuracy of the DGPS-based position solution. The data collected indicated that pseudorange and pseudorange-rate difference corrections having an age greater than approximately 20 sec resulted in significantly larger errors. All of the data collected was accomplished with pseudorange and pseudorange-rate difference corrections having an age greater than five sec, with a majority of the data collected having pseudorange and pseudorange-rate difference corrections less than 10 sec in age.

Figure 21 shows that the vertical position error bounds for the 6° glideslope approaches converge and diverge at approximately 6500 m and again at approximately 3000 m. No correlation could be made between either the satellite geometry or age of the pseudorange and pseudorange-rate difference corrections and the increase followed by the decrease in positioning accuracy at these ranges.

Figure 23 shows that the vertical position error bounds for the 9° glideslope approaches converge and diverge at approximately 2500 m. Again, no correlation could be made between either the satellite geometry or age of the pseudorange and pseudorange-rate difference corrections and the increase followed by the decrease in positioning accuracy at this range.
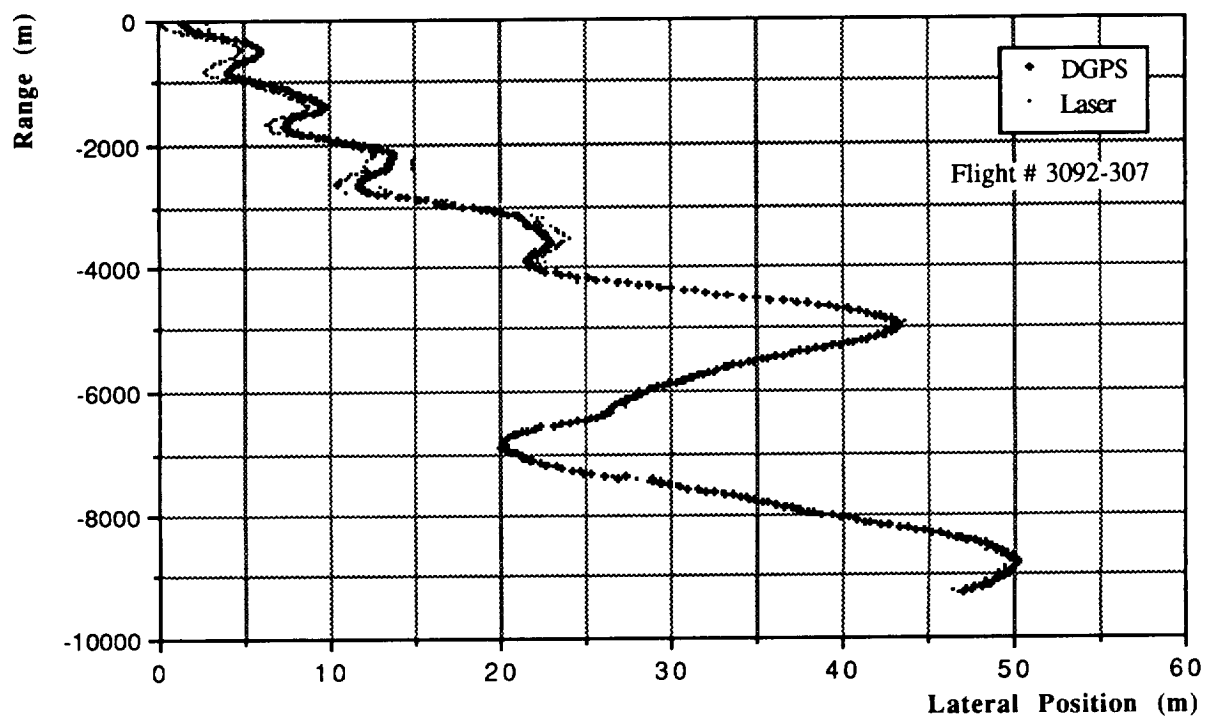
Figure 14

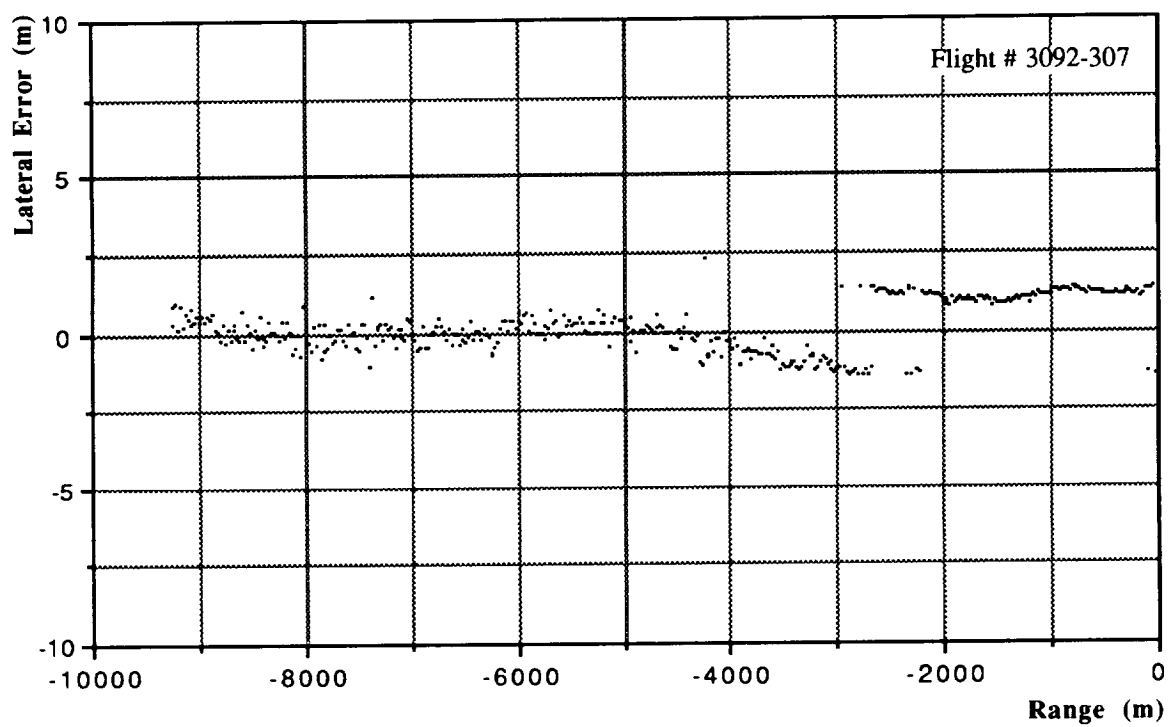Sample 3° Glideslope Approach Lateral Position

Figure 15

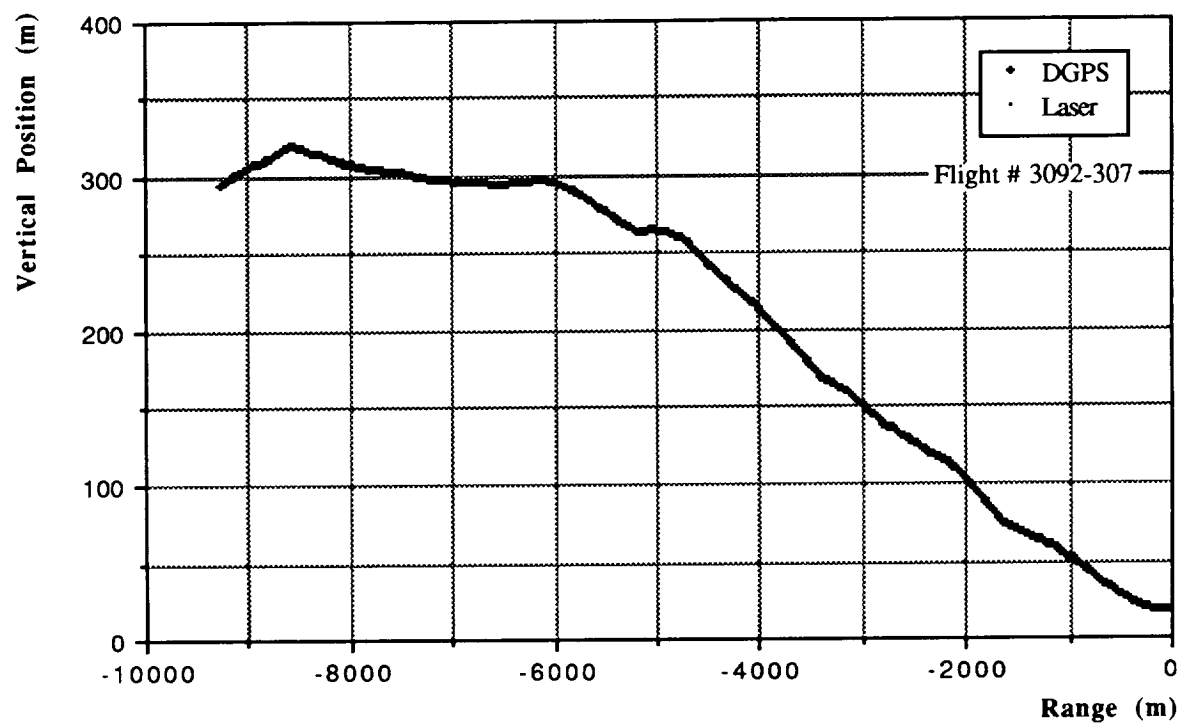Sample 3° Glideslope Approach Lateral Position Error

Figure 16

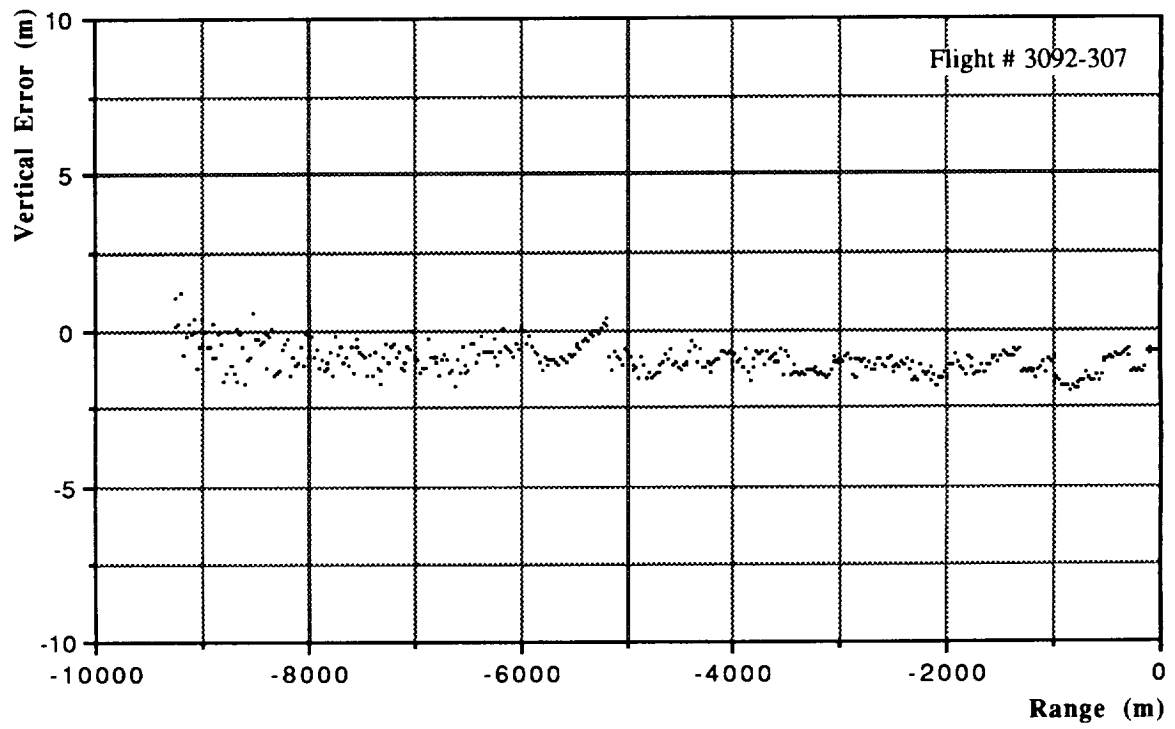Sample 3° Glideslope Approach Vertical Position

Figure 17

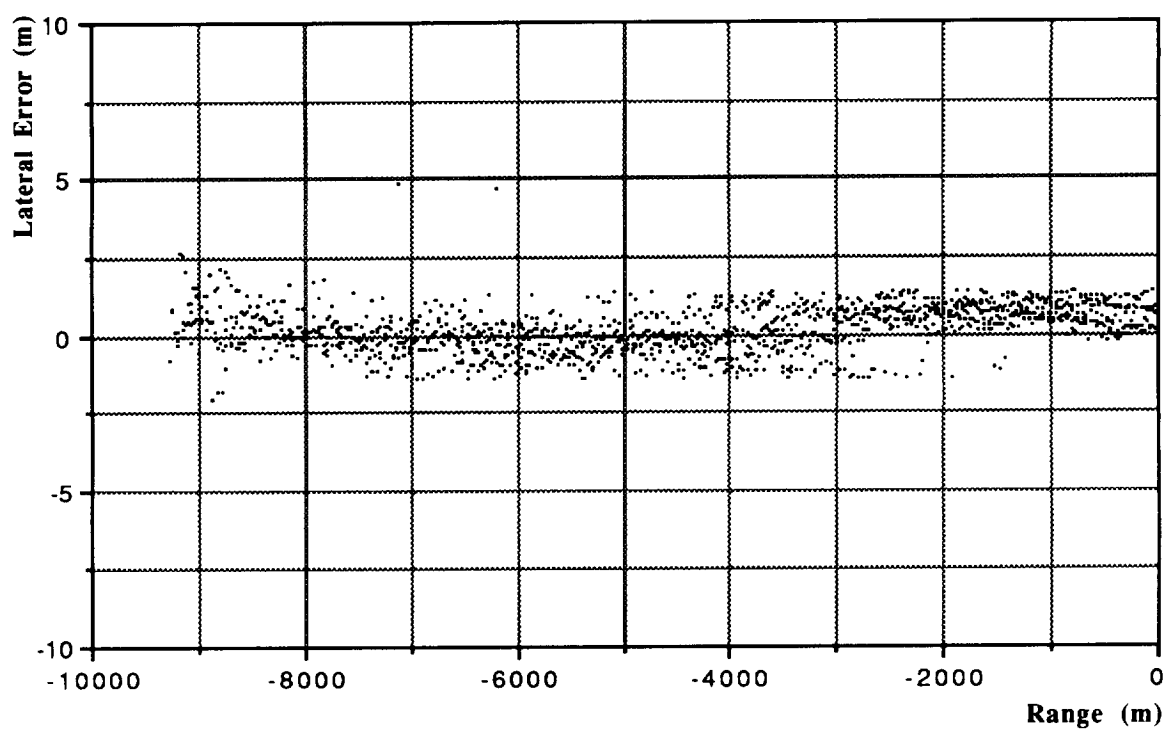Sample 3° Glideslope Approach Vertical Position Error

Figure 18

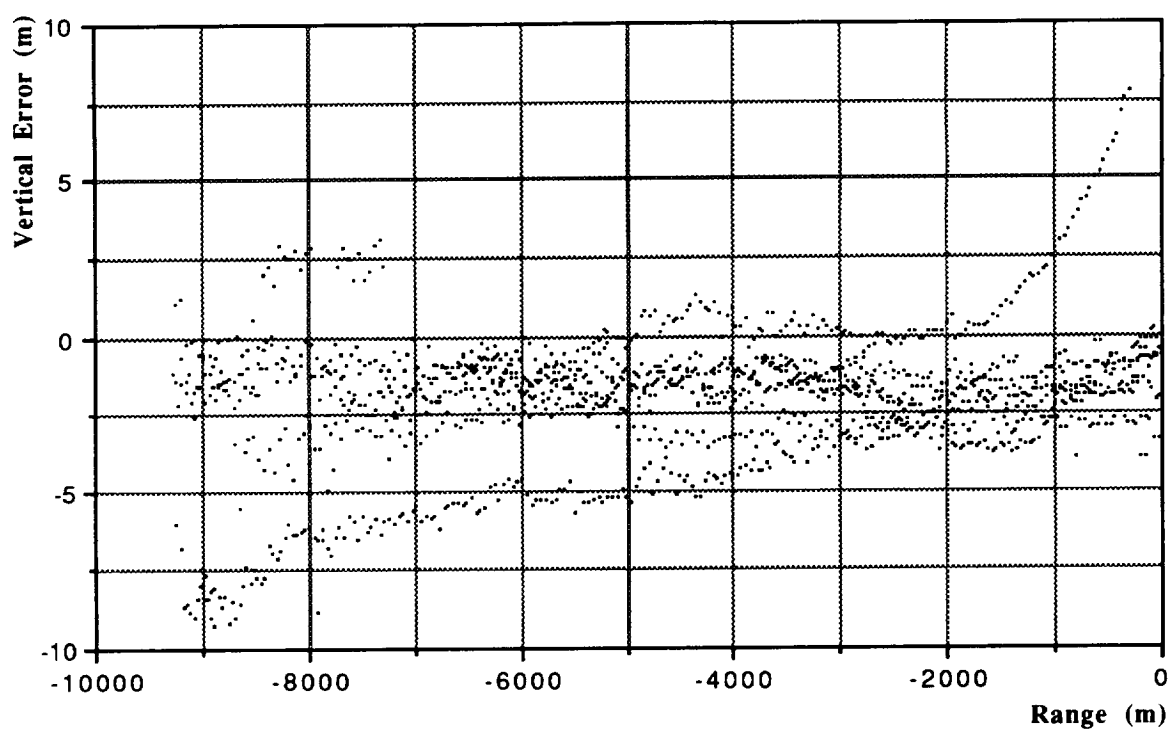Composite 3° Glideslope Approach Lateral Position Error

Figure 19

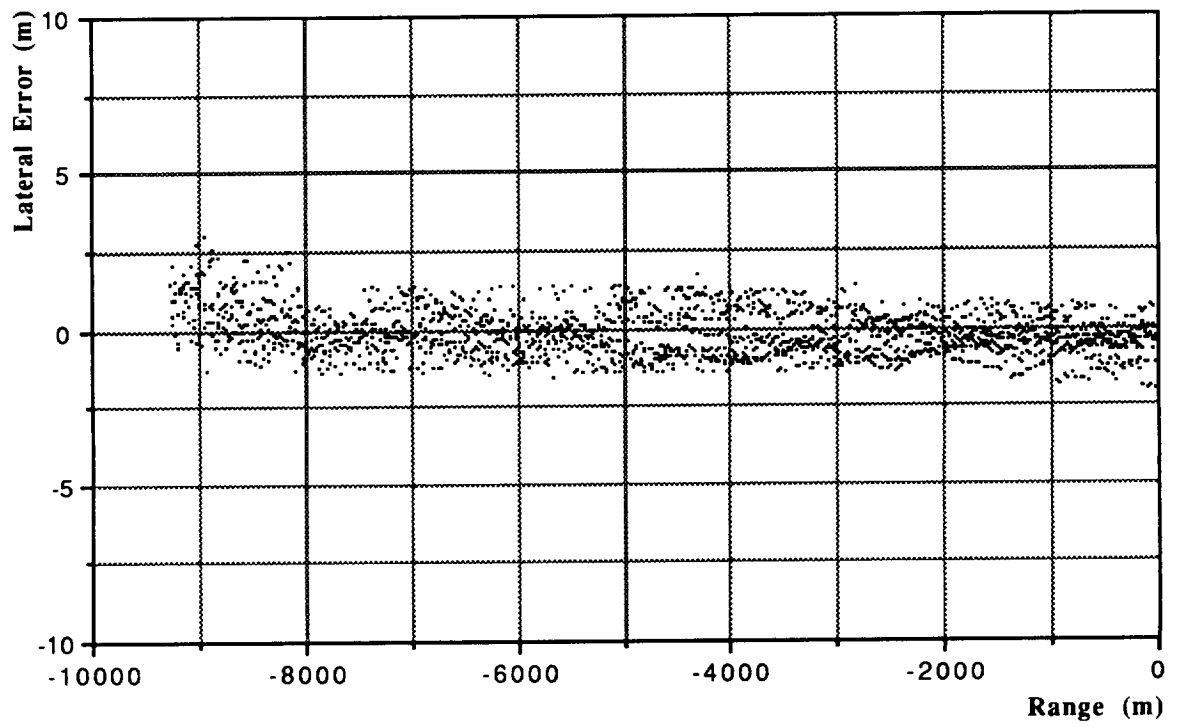Composite 3° Glideslope Approach Vertical Position Error

Figure 20

Composite 6° Glideslope Approach Lateral Position Error
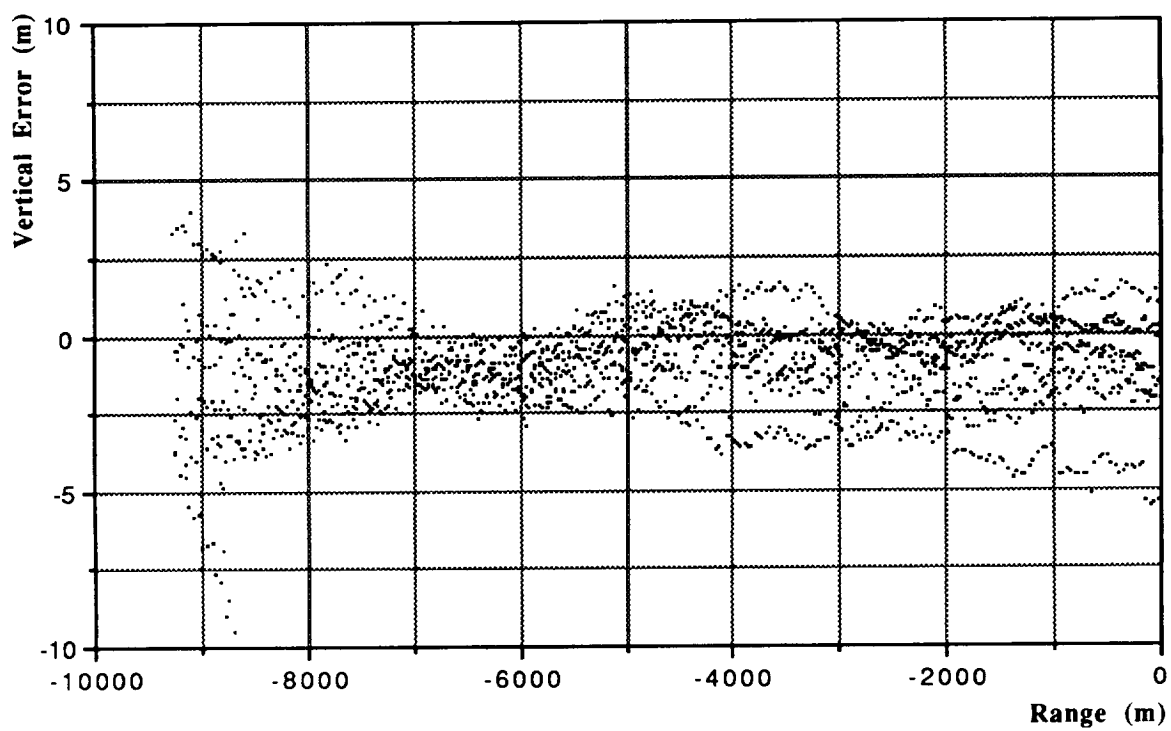
Figure 21

Composite 6° Glideslope Approach Vertical Position Error
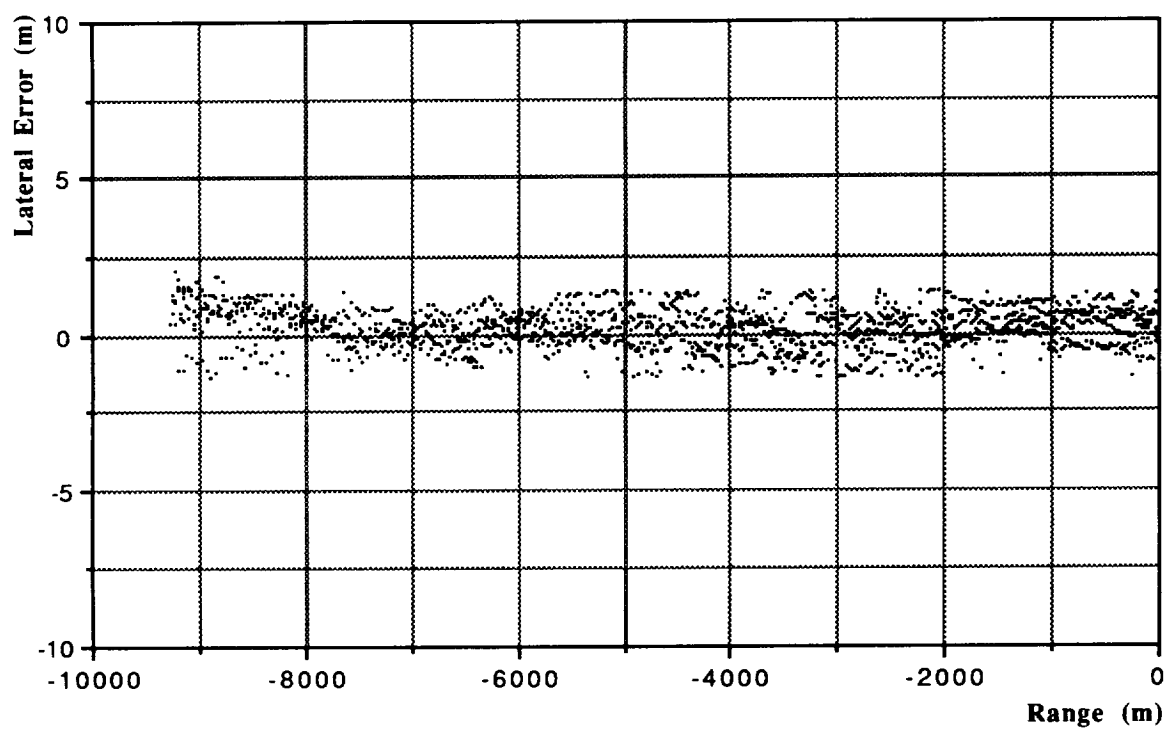
Figure 22

Composite 9° Glideslope Approach Lateral Position Error
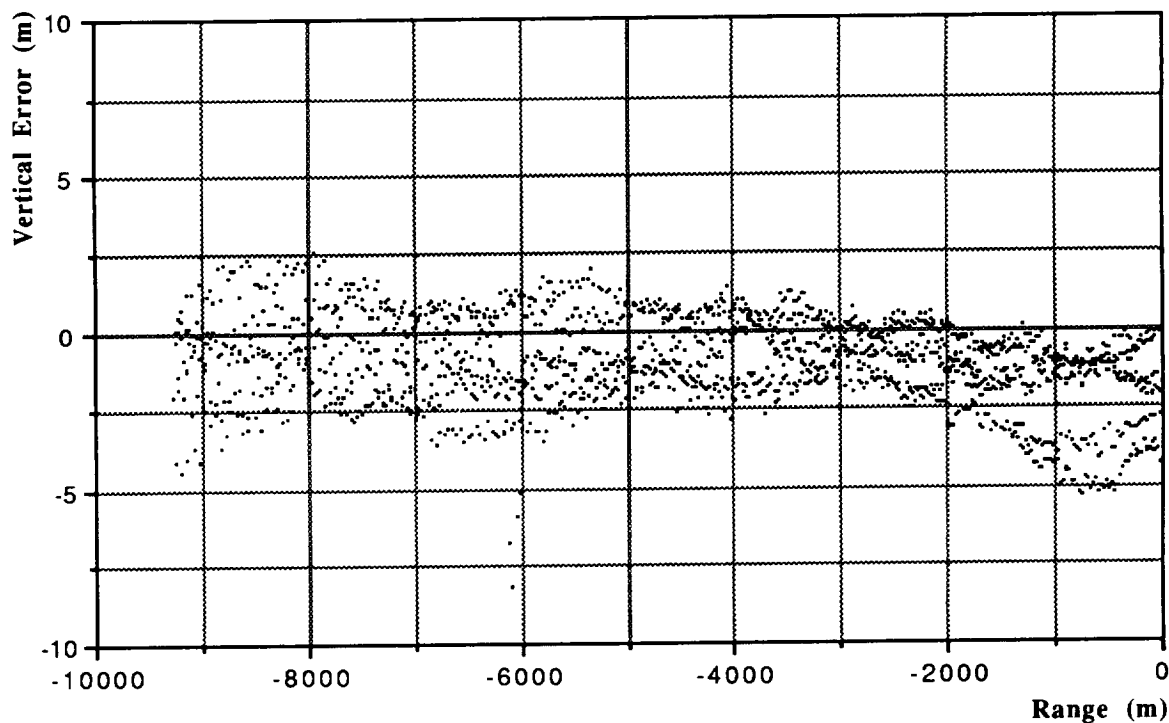
Figure 23

Composite 9° Glideslope Approach Vertical Position Error

Time histories of the position errors were calculated at a rate of 2 Hz. A time history analysis assumes that the DGPS positioning accuracy is not a function of the aircraft position during the approach. Therefore, all of the data collected for each approach is given equal weighting in the statistical analysis. The composite position error statistics for each of the three types of approaches flown are summarized in Table 1.

Table 1

Composite Position Error Statistics For Each Type of Approach

Error Orientation	3° Approach Error (m)		6° Approach Error (m)		9° Approach Error (m)	
	Mean	SD (2σ)	Mean	SD (2σ)	Mean	SD (2σ)
Longitudinal	-0.79	±2.74	-1.38	±3.95	-0.73	±2.51
Lateral	+0.22	±1.78	-0.14	±1.47	+0.18	±1.27
Vertical	-2.03	±3.54	-1.08	±3.51	-0.99	±2.81

Since the longitudinal mean position error is biased in the opposite direction of aircraft motion for all of the approaches and is significantly larger than the lateral mean position error, it appears to be a result of computational time lags within the DGPS receiver, which in turn increases the age of the pseudorange and pseudorange-rate difference corrections. Such computational time lags were noticed at the ground-based DGPS receiver during the uplinking of the pseudorange and pseudorange-rate difference corrections to the aircraft. As the number of satellites that the ground-based DGPS receiver tracked increased, the rate at which the pseudorange and pseudorange-rate difference corrections were calculated and transmitted decreased. It should be noted that longitudinal mean position error is not as critical as lateral and vertical mean position errors during approaches to landing. The lateral mean position errors are relatively small, as would be expected. The vertical mean position errors are significantly larger than the lateral mean position errors and are primarily due to the uncertainty in the DGPS vertical solution, and possibly due in part to a bias due to the age of the pseudorange and pseudorange-rate difference corrections.

The lateral and vertical position errors show an increase in accuracy as the glideslope increases (See Table 1). This is possibly due to the fact that the steeper the approach, the

slower the airspeed and therefore the greater the number of data points to analyze, with the result being a more statistically accurate analysis.

The next analysis performed was a decision height analysis, where only data points corresponding to the 200 ft DH on a standard 3° glideslope approach were used. This type of analysis is typically used in evaluating the navigational accuracy of approach and landing systems. The position errors at the 200 ft DH for six of the seven 3° glideslope approaches flown (excluding flight number 3092-308 due to the interruption of the pseudorange and pseudorange-rate difference corrections at the DH) are summarized in Table 2, as well as Figures 24 and 25.

Table 2

Position Error Statistics At The 3° Approach 200 ft Decision Height

Error Orientation	200 ft DH Error (m)	
	Mean	SD (2σ)
Longitudinal	-0.61	±2.79
Lateral	+0.34	±1.49
Vertical	-2.25	±1.63

The results indicate improvement in position accuracy at the 200 ft DH as compared to the time history analysis results for the entire approach. Again this might be due to the increased accuracy of the laser at shorter ranges. However, it should be noted that the decision height analysis is based on only six data points from six 3° approaches flown.
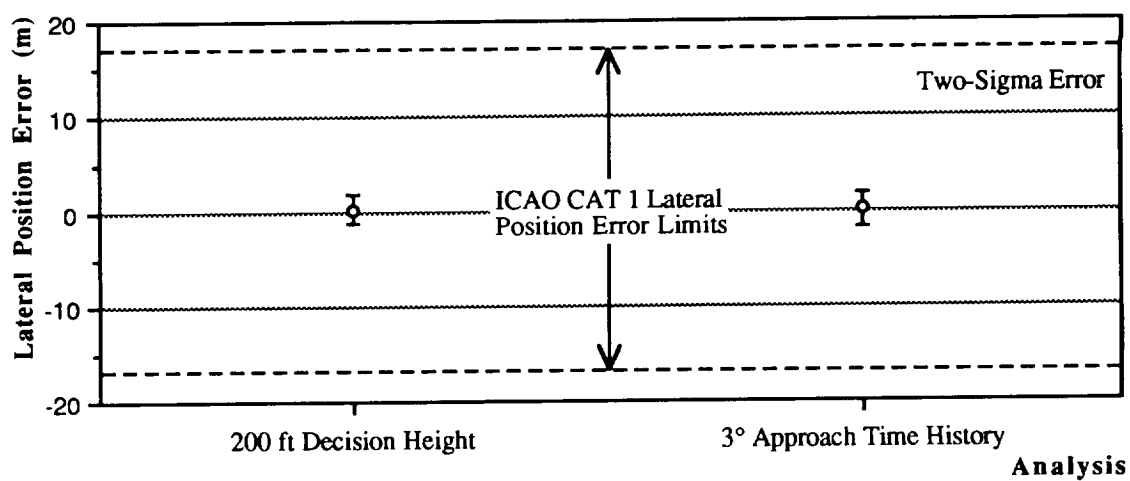
Figure 24

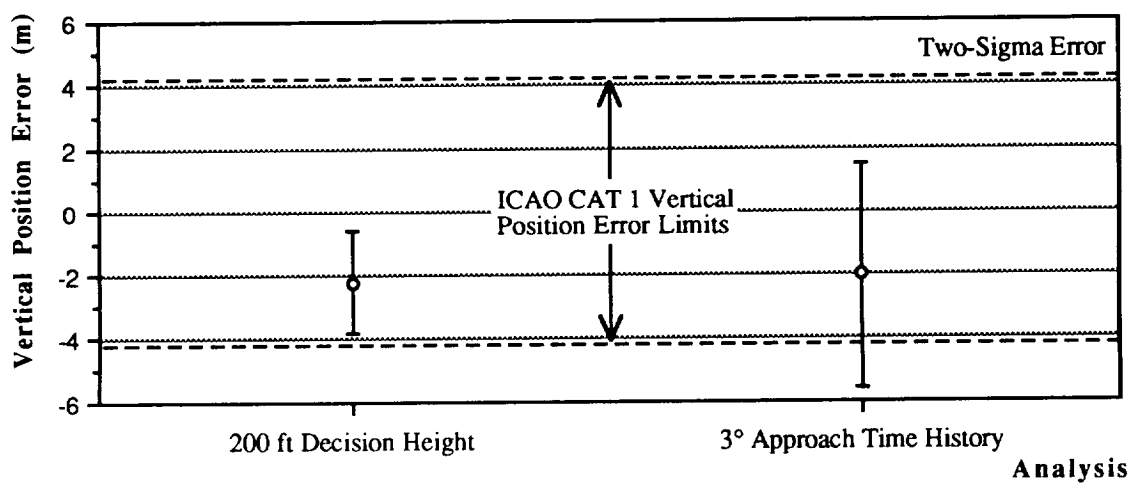3° Glideslope Approach Lateral Position Error Statistics

Figure 25
3° Glideslope Approach Vertical Position Error Statistics

CHAPTER 6

Conclusions

<u>Accuracy Considerations</u>

DGPS positioning accuracy is composed of lateral and vertical error components. The accuracy requirements for a precision approach can be expressed in terms of lateral and vertical error limits. A comparison of DGPS accuracy with respect to the precision approach requirements provides an indication of the feasibility of using DGPS to provide high accuracy, precision navigation and guidance for helicopter precision approaches to landing.

<u>Precision Approach Requirements For A 3° Glideslope</u>

The point at which the 3° glideslope is 200 ft above the surface is defined by ICAO to be the CAT 1 DH point [12]. The DH is defined by FAA Order 8260.3B (U.S. Standard for Terminal Instrument Procedures) to be the height, specified in feet above MSL, above the highest elevation in the touchdown zone at which a missed approach shall be initiated if the required visual reference has not been established.

The lateral requirement at the CAT 1 DH point is ±17.1 m (2σ) and the vertical precision approach accuracy requirement is 4.2 m (2σ) [12]. These accuracy requirements are based on ICAO ILS standards for ground equipment and assume a 3° glideslope and 8000 ft distance between the localizer antenna and the runway threshold.

<u>Comparative Assessment</u>

DGPS positioning accuracy at the 200 ft DH on a standard 3° glideslope approach was 0.3 m (mean) ±1.5 m (2σ) laterally and -2.3 m (mean) ±1.6 m (2σ) vertically. These errors indicate that the helicopter position based on DGPS guidance satisfies the ICAO CAT 1 lateral and vertical navigational accuracy requirements (See Figures 24 and 25). Note that these results are based upon a limited set of data (six data points from six approaches). The relatively large vertical mean error is due primarily to the uncertainty

in the DGPS vertical solution. In addition, the vertical mean error may be due in part to a bias due to the age of the pseudorange and pseudorange-rate difference corrections.

Concluding Remarks

The DGPS system utilized commercial receivers designed primarily for land surveying applications and was compatible with the ILS type localizer and glideslope instruments onboard the NASA UH-60 helicopter. Pilots commented that the DGPS-based guidance appeared smooth, accurate and easy to follow.

The decision height analysis revealed that the DGPS system did achieve ICAO CAT 1 navigational accuracy requirements for a standard 3° glideslope approach. In addition, 14 of the 21 approaches analyzed using the time history analysis also displayed sufficient navigational accuracy to meet such requirements. This is a significant result, since all previous research, conducted with DGPS only, has not achieved such accuracy. One reason for this is the rapid technological advancement made in both hardware and software design currently available in DGPS receivers.

The age of the pseudorange and pseudorange-rate difference corrections has a significant impact on the accuracy of the DGPS position solution. A bias due to the age of the pseudorange and pseudorange-rate difference corrections may contribute to the vertical position error, and to a lesser extent to the longitudinal and lateral position error.

CHAPTER 7

Recommendations

The age of the pseudorange and pseudorange-rate difference corrections needs to be monitored and a warning needs to be displayed to the pilot when this age becomes greater than 20 sec. The results of this research indicated that the positioning accuracy started to deteriorate significantly after a 20 sec, or more, interruption of the pseudorange and pseudorange-rate difference corrections.

The guidance and navigation algorithms can be modified to increase the positioning accuracy. This is accomplished by integrating the DGPS and INS via Kalman filtering techniques. This integration is the subject of current research at the NASA Ames Research Center to improve helicopter precision guidance and navigation.

In order to take advantage of the improved positioning accuracy provided by the DGPS/INS integration, which in turn may allow flying to a lower DH, a more sophisticated display is needed to indicate localizer and glideslope deviation. Such a display would need to provide a more accurate and timely indication of the localizer and glideslope deviations, which would be required to fly to a lower DH.

LIST OF REFERENCES

1. Milliken, R.J. and Zoller, C.J.
    "Principle Operation of NAVSTAR and System Characteristics"
    Navigation: Journal of the Institute of Navigation, Vol. 25, No. 2, Summer 1978

2. Ellowitz, H.I.
    "The Global Positioning System"
    Microwave Journal, April 1992

3. Langley, R.B.
    "The Mathematics of GPS"
    GPS World Magazine, July/August 1991

4. Edwards, F.G. and Loomis, P.V.W.
    "Civil Helicopter Flight Operations Using Differential GPS"
    Navigation: Journal of the Institute of Navigation, Vol. 32, No. 3, Fall 1985

5. Edwards, F.G., Paielli, R.A. and Hegarty, D.M.
    "Helicopter Terminal Approach Using Differential GPS with Vertical-Axis Enhancement"
    Satellite Division Meeting of the Institute of Navigation, Colorado Springs, CO September 1987

6. Edwards, F.G., Hegarty, D.M., Turner, R.N., van Grass, F. and Sharma, S.
    "Validating the Airborne and Ground Based Components of a Differential GPS System"
    National Technical Meeting of the Institute of Navigation, Santa Barbara, CA, Janurary 1988

7. Edwards, F.G. and Hegarty, D.M.
    "Flight Test Evaluation of Civil Helicopter Terminal Approach Operations Using Differential GPS"
    AIAA 89-3635, AIAA Guidance, Navigation and Control Conference, Boston, MA, August 1989

8. McNally, D.B., Warner, D.N., Hegarty, D.M. and Schultz, T.A.
    "Flight Evaluation of Precision Code Differential GPS for Terminal Area Positioning"
    Proceedings of the Fourth International Technical Meeting of the Satellite Division of the Institute of Navigation (ION GPS-91), Albuquerque, New Mexico, September 1991

9. MacDonald, S.L. and Clary, G.R.
    "Operations Manual for the LILS Interface"
    Sierra Nevada Corporation, September 1985

10. Leick, A.
    "Geometric Geodesy, 3-D-Geodesy and Conformal Mapping"
    University of Maine, Department of Surveying Engineering, 1980

11. Peach, L.L., Jr., Bull, J.S., Anderson, D.J., Dugan, D.C., Ross, V.L., Hunting, A.W., Pate, D.P. and Savage, J.C.
    "NASA/FAA Flight-Test Investigation of Helicopter Microwave Landing System Approaches"
    Preprint Number 80-55, American Helicopter Society 36th Annual Forum, Washington, D.C., May 1980

12. Hogle, L.
    "Investigation of the Potential Application of GPS for Precision Approaches"
    Navigation: Journal of the Institute of Navigation, Vol. 35, No. 3, Fall 1988